



# Crystal packing, vibrational studies, DFT calculations of a new hybrid nickel (II)-complex and its application in Heck and Sonogashira cross-coupling reactions

Rim Jaballi<sup>1</sup> | Wassim Maalej<sup>1</sup> | Dhieb Atoui<sup>2</sup> | Habib Feki<sup>3</sup> | Ridha Ben Salem<sup>2</sup> | Zakaria Elaoud<sup>1</sup>

<sup>1</sup>Laboratory of Physical and Chemistry of Solid State, University of Sfax, Faculty of Sciences of Sfax, Tunisia

<sup>2</sup>Organic Chemistry Laboratory (LR17/ES08), University of Sfax, Faculty of Sciences of Sfax, Tunisia

<sup>3</sup>Laboratory of Applied Physics (LAP), University of Sfax, Faculty of Sciences of Sfax, Tunisia

## Correspondence

Wassim Maalej, Sfax Faculty of Sciences, Chemistry Department, Soukra Road km 3,5 - B.P. 1171, 3018 Sfax - Tunisia.  
Email: maalej\_wassim@yahoo.fr

We particularly investigate a new material  $[\text{Ni}(\text{C}_{12}\text{H}_{12}\text{N}_2)(\text{H}_2\text{O})_4]\text{SO}_4$  that it was hydrothermally synthesized by reaction of 5,5'-dimethyl-2,2'-bipyridine, denoted (dmbpy), metal salt and sulfuric acid. The large crystals are characterized by X-ray single crystal diffraction, infrared, Raman spectroscopy and DFT calculation. The thermogravimetric analysis indicated that the dehydration occurs in two steps, leading to an anhydrous compound. At room temperature, the complex crystallises in the centrosymmetric space group  $P2_1/c$  with the following parameters  $a = 9.492(7) \text{ \AA}$ ,  $b = 9.539(7) \text{ \AA}$ ,  $c = 18.411(1) \text{ \AA}$ ,  $\beta = 102.616(1)^\circ$ ,  $V = 1626.8(2) \text{ \AA}^3$  and  $Z = 4$ . The asymmetric unit contains one free  $\text{SO}_4^{2-}$  counter-ion and  $[\text{Ni}(\text{dmbpy})(\text{H}_2\text{O})_4]^{2+}$  complex cation. The crystal structure of the complex is built up from infinite parallel two-dimensional planes, containing all the components of the structure and perpendicular to the axis  $b$ . The aqua ligands are connected to the sulfate anion via O-H...O hydrogen bonds that stabilize the three-dimensional network.

The catalytic activity of the complex was examined in the coupling reactions of Heck and Sonogashira in the presence of different bases in various organic solvents under ultrasonic irradiation. The obtained results show that this type of complex can be considered as an effective catalyst for these coupling reactions. The ultrasonic activation results the encouraging yields for a short period of time: 30-45 min.

## KEYWORDS

Catalyst, Coupling reaction, Crystal structure, Ultrasonic activation, X-ray diffraction

## 1 | INTRODUCTION

Inorganic-organic hybrid materials have recently received much attention due to their fascinating structural diversities,<sup>[1-4]</sup> i.e. not only for the structures and properties of coordination complexes, but also for their excellent physical properties, such as magnetic, ferroelastic, nonlinear optical activity, and electrical properties.<sup>[5-7]</sup> A large

number of these materials are prepared in the presence of pyridine and their derivatives (5,5'-dimethyl-2,2'-bipyridine, phenantroline, 4,4'-dimethyl-2,2'-bipyridine...)<sup>[8-10]</sup> Particularly, studies of hybrid compound based on nickel have become an active research area in organic chemistry, biology and crystal.<sup>[2,11]</sup> Thus, in recent years, certain catalytic processes have been developed.<sup>[12,13]</sup> Among the different strategies, the uses

of N,N'-bidentate ligand complexes have been proposed. Out of the ligands developed, several examples of 2, 2'-bipyridines,<sup>[14–16]</sup> 1, 10'-phenanthrolines<sup>[17,18]</sup> and recently the iminopyridines<sup>[19]</sup> were examined. This type of complex is currently attracting much attention for industrial and academic research teams.<sup>[20]</sup> In fact, it acts as a catalyst for various currently important chemical reactions. The Kocovsky and Malkov groups have reported that Cu (I) complexes of 2,2'-bipyridines are very efficient catalysts for the allylic oxidation of olefins.<sup>[21]</sup> Similar results have recently displayed that the O-arylation of phenols and aliphatic alcohols with the aryl halides can be carried out in good yield.<sup>[22]</sup> Other studies have examined new complexes of nickel (II) dibromide of N, N'-bidentate ligands containing pyrazole (pz), pyrimidine ( $\mu\text{m}$ ) or pyridine (py) aromatic rings.<sup>[23]</sup> These complexes were tested as catalysts for the polymerization of ethylene resulting from moderate to high activities.

In the present work, we describe the chemical preparation, the crystal structure, and the thermal analyses. Moreover, we report the combined experimental and theoretical vibration and the convergence between them of a new compound. We also examined their catalytic activity in Heck and Sonogashira coupling reactions. The catalytic tests were studied using different bases in various organic solvents under ultrasonic irradiation although it is considered the best economical and ecological alternative for the rapid activation of the chemical reaction.

## 2 | EXPERIMENTAL DETAILS

### 2.1 | Chemical preparation

#### 2.1.1 | Synthesis of $[\text{Ni}(\text{C}_{12}\text{H}_{12}\text{N}_2)(\text{H}_2\text{O})_4]\text{SO}_4$ crystal

The crystal was synthesized hydrothermally from a mixture, nickel (II) nitrate hexahydrate (0.5 mmol, 0.14 g) dissolved in 5 ml water, 5,5'-dimethyl-2,2'-bipyridine (1 mmol, 0.18 g) dissolved in 7 ml MeCN and sulfuric acid (0.13 ml, 2 M).



The mixture was transferred to a Teflon-lined autoclave and heated at 413 K, for 3 days. A large and blue sample of the dimensions 0.500 x 0.400 x 0.300 mm were collected by filtration, washed with water before being dried at room temperature, and then cut and selected for single-crystal X-ray experiments. The percentages of organic elemental analysis CHNOS of  $[\text{Ni}(\text{dmbpy})(\text{H}_2\text{O})_4]\text{SO}_4$  are given in Figure 1.

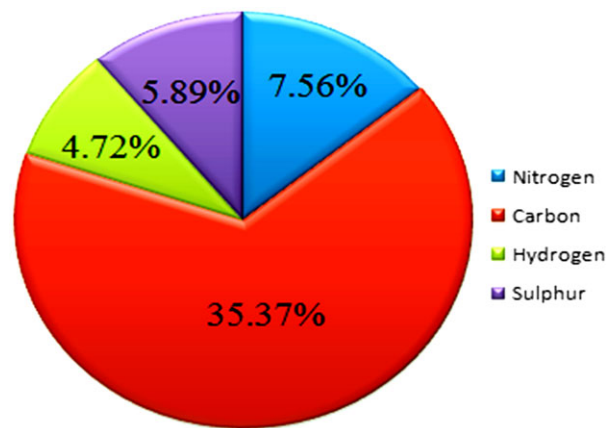


**FIGURE 1** The elemental analysis of the  $[\text{Ni}(\text{C}_{12}\text{H}_{12}\text{N}_2)(\text{H}_2\text{O})_4]\text{SO}_4$

#### 2.1.2 | General Procedure for Heck Cross-Coupling Reaction:

The reactor (beaker of 25 ml) was charged with 0.012 mmol of catalyst, 1.5 mmol of base, 1 mmol of aryl halide, 1 mmol of styrene and 6 ml of the solvent were finally added to the mixture obtained and subjected to ultrasonic irradiation, at room temperature (25 °C). After the reaction, the mixture was cooled and the organic phase extracted with n-hexane and then with the saturated NaCl solution. The adduct obtained was then dried using  $\text{Na}_2\text{SO}_4$  and filtered. The solvent was evaporated using a rotary evaporator.

#### 2.1.3 | General Procedure for Sonogashira Cross-Coupling Reaction:

The reactor (beaker of 25 ml) was charged with 0.012 mmol of catalyst, 1.5 mmol of base, 1 mmol of aryl halide, 1 mmol of phenylacetylene and 6 ml of the solvent were finally added. The mixture obtained was subjected to ultrasonic irradiation, at room temperature (25 °C). After the reaction, the mixture was cooled and we followed the same procedure of extraction, filtration and purification regarding Heck coupling reaction.

### 2.2 | X-ray data collection

Single-crystal X-ray diffraction intensity data were collected at 293(2) K with a Bruker smart sApex CCD diffractometer using Mo-K $\alpha$  radiation ( $\lambda = 0.71073 \text{ \AA}$ ). The data were collected at room temperature. Lorentz and polarizing effect corrections were performed before proceeding to the refinement of the structure. Besides, absorption corrections were performed using the multi-scan technique and the atomic scattering factors were taken from the International Tables for X-ray Crystallography.<sup>[24]</sup> 3102

independent reflections were measured, 2551 of which had an intensity of  $I > 2\sigma(I)$ . The structure analyses were carried out with the monoclinic symmetry,  $P2_1/c$  space group, according to the automated search for the space group available in WINGX.<sup>[25]</sup> The sulfur atoms and transition metal “Ni” were fixed using the Patterson methods with SHELXS-86 program.<sup>[26]</sup> Nitrogen, carbon and oxygen atoms were found from successive Fourier calculations using SHELXL-97.<sup>[27]</sup> The water H atoms were located in a difference map and refined with O-H distance restraints of 0.88(2) Å and H-H restraints of 1.5(2) Å. H atoms bonded to C atoms were positioned geometrically and allowed to ride on their parent atoms, with C-H bonds fixed at 0.97 Å. The final cycle of refinement led to the final reliability factors  $R_1 = 0.047$  and  $wR_2 = 0.120$ . Moreover, the drawings were made with Diamond.<sup>[28]</sup>

The Crystallographic data and structure refinement details for  $[\text{Ni}(\text{C}_{12}\text{H}_{12}\text{N}_2)(\text{H}_2\text{O})_4]\text{SO}_4$  are summarized in Table 1. The hydrogen bonds are listed in Table 2. The Fractional atomic coordinates and isotropic or equivalent isotropic displacement parameters, atomic displacement parameters and the interatomic distances and bonds angles are given in Tables 3, 4 and 5, respectively.

### 2.3 | Differential scanning calorimetry (DSC) and thermogravimetric analysis (TGA)

Thermogravimetric analysis and Differential scanning calorimetry for  $[\text{Ni}(\text{C}_{12}\text{H}_{12}\text{N}_2)(\text{H}_2\text{O})_4]\text{SO}_4$  were carried out with NETZSCH STA 449F1 instrument. The 27.5 mg powdered sample was spread evenly in a large sample holder to avoid mass effect, in the temperature range 20–500 °C. The TG run was performed in following air with a heating rate of 5 °C/min<sup>-1</sup>.

### 2.4 | Powder X-ray diffraction

Concerning the phase analysis, the X-Ray powder patterns were recorded in the 2THETA range 10–80° using a Siemens D5000 powder diffractometer with Cu-K $\alpha$  radiation ( $\lambda$  (K $\alpha$ ) = 1.5406 Å) selected with a diffracted-beam graphite monochromator. Powder X-ray diffraction was employed to verify that the materials used for thermal analyses were the same phase as the single crystal structures for the new complex.

### 2.5 | Spectroscopic measurements

The FT-IR and FT-Raman spectra of the compound  $[\text{Ni}(\text{C}_{12}\text{H}_{12}\text{N}_2)(\text{H}_2\text{O})_4]\text{SO}_4$  were investigated in the frequency range 400–4000 cm<sup>-1</sup>. Raman scattering was

**TABLE 1** Crystal data and structure refinement

Color/Shape	Blue/Parallelepipedic
Formula	$[\text{Ni}(\text{C}_{12}\text{H}_{12}\text{N}_2)(\text{H}_2\text{O})_4]\text{SO}_4$
Mr (g mol <sup>-1</sup> )	411.05
Crystal system	Monoclinic
Space group	$P2_1/c$
Temperature (K)	293(2)
a (Å)	9.4920 (7)
b (Å)	9.5392 (7)
c (Å)	18.4113 (11)
$\beta$ (°)	102.616 (4)
Volume(Å <sup>3</sup> )	1626.8 (2)
Z-space group	4
F (000)	856
Crystal dimensions (mm <sup>3</sup> )	0.50 × 0.40 × 0.30
Diffractometer	CCD area detector
$\theta$ range for data collection (deg)	2.3 < $\theta$ < 27.5
Radiation, $\lambda$ (Å), monochromator	Mo K $\alpha$ , 0.71073, graphite
Observed reflections $I > 2\sigma(I)$	2551
$R_{\text{int}}$	0.031
Range of h, k, l	-11/10, -12/11, -23/23
Refined parameters	274
goodness of fit	1.19
Final R	0.047
Rw	0.120
W	$=1/[\sigma^2(F_o^2) + (0.0188P)^2 + 6.1771P]$ $P = (F_o^2 + 2F_c^2)/3$

performed at room temperature using a LABRAM-Jobin Yvon set up. The excitation line was the 630 nm from a Neon laser. The incident laser power was limited to 5 mW to avoid sample heating degradation. The laser beam was focused onto the sample through a 50 x microscope objective. Furthermore, Infrared measurements were obtained using a Perkin-Elmer FT-IR Spectrum and the samples were diluted with spectroscopic grade KBr and pressed into a pellet. All the bonds were assigned by comparison with the spectrum of other compounds, at room temperature. The frequencies for the corresponding bonds are given in Table 6.

The UV–Visible absorption spectrum was recorded at room temperature using a Lambda 1050 UV/Vis/NIR spectrometer within the range of 200–800 nm. BaSO<sub>4</sub> was used as a reference material.

The <sup>1</sup>H NMR and <sup>13</sup>C NMR spectra of the synthesized compounds were recorded on a Bruker AC 400 apparatus

**TABLE 2** Hydrogen-bond geometry (Å, °)

D—H...A	D—H	H...A	D...A	D—H...A
O1W—H1WA...O3 <sup>i</sup>	0.80 (6)	1.89 (6)	2.688 (5)	174 (6)
O1W—H1WB...O4	0.77 (6)	1.95 (7)	2.723 (5)	175 (6)
O2W—H2WA...O3	0.70 (6)	2.12 (7)	2.798 (5)	164 (7)
O2W—H2WB...O4 <sup>ii</sup>	0.84 (7)	1.92 (7)	2.744 (5)	168 (6)
O3W—H3WA...O1 <sup>iii</sup>	0.69 (7)	2.08 (7)	2.769 (6)	174 (7)
O3W—H3WB...O2 <sup>i</sup>	0.86 (7)	1.97 (7)	2.824 (5)	171 (6)
O4W—H4WB...O1 <sup>ii</sup>	0.86 (8)	1.91 (8)	2.761 (5)	177 (7)
O4W—H4WA...O2 <sup>iii</sup>	0.65 (8)	2.06 (8)	2.711 (6)	177 (9)

Symmetry codes: (i)  $-x+2, y-1/2, -z+3/2$ ; (ii)  $-x+2, y+1/2, -z+3/2$ ; (iii)  $x-1, y, z$ ; (iv)  $-x+2, -y, -z+2$ .

with Fourier transform and a nominal frequency of 100 MHz. Chemical shifts are expressed in parts per million (ppm) relative to tetramethylsilane (TMS), used as an internal reference.

The yields were measured by gas chromatography on a Shimadzu 2014-GC apparatus using dichloromethane as solvent. The capillary column was DB-5 and the carrier gas was nitrogen.

## 2.6 | Theoretical calculations

The vibrational wavenumber calculations and molecular geometry optimization carried out in the present work were recorded by DFT method employing the Gaussian 09 package. The Becke three-parameter hybrid exchange functional and the Lee-Yang-Parr correlation functional (B3LYP) were used in the calculation with the LanL2DZ basis set.<sup>[29]</sup>

## 2.7 | Ultrasonic activation:

Irradiation was guaranteed by using an ultrasonic probe (Sonopuls HD 3200 model, 20 kHz, 200 W) with an ultrasonic generator (Sonics VC 505, 300 W). The ultrasonic probe ( $\Phi = 3$  mm) was immersed directly in the reactor. The sonication was carried out at a low frequency of 20 kHz (amplitude of 40%) at room temperature with a 3-s pulsation.

## 3 | RESULTS AND DISCUSSION

### 3.1 | Structure description

A molecular view of complex  $[\text{Ni}(\text{C}_{12}\text{H}_{12}\text{N}_2)(\text{H}_2\text{O})_4]\text{SO}_4$  is shown in Figure (2a). The basic unit of the studied material is made up of one  $[\text{Ni}(\text{dmbpy})(\text{H}_2\text{O})_4]^{2+}$  cation and one  $[\text{SO}_4]^{2-}$  anion. The corresponding optimized geometry by the DFT calculation is shown in Figure (2b). A

prismatic crystal obtained was selected by optical examination using a polarized microscope. This complex crystallises in the monoclinic  $P2_1/c$  system with the following unit cell dimensions  $a = 9.492$  (7) Å,  $b = 9.539$  (7) Å,  $c = 18.411$  (1) Å,  $\beta = 102.616^\circ$  (1),  $V = 1626.8$  (2) Å<sup>3</sup> and  $Z = 4$ .

Examination of the structure shows a layer arrangement perpendicular to  $c$  axis: planes of Octahedron alternate with planes of  $\text{C}_{12}\text{H}_{12}\text{N}_2$ . The  $[\text{Ni}(\text{dmbpy})(\text{H}_2\text{O})_4]^{2+}$  unit possesses a configuration of distorted octahedral so that the central Nickel (II) ion is surrounded by four oxygen and two nitrogen atoms. The equatorial plane of the octahedron is formed by a pair of nitrogen donor from dmbpy ligand and two molecules of water (O2, O3), while the two remaining water molecules (O1, O4) coordinate at the axial sites. The Ni-O and Ni-N bond length are almost equivalent (Ni-N1 = 2.065(3), Ni-N2 = 2.058(4), Ni-O2W = 2.063(3) and Ni-O3W = 2.061(4) Å), but Ni-O1W (2.023(3)) and Ni-O4W (2.032(4)) are shorter than the others. This is one of the main factors accounting for the distortion from the ideal octahedral geometry of the  $\text{Ni}^{\text{II}}$  center; this is due to the heterogeneous environment and the Jahn Teller effect. Bond lengths and angles within the octahedron  $[\text{Ni}(\text{C}_{12}\text{H}_{12}\text{N}_2)(\text{H}_2\text{O})_4]^{2+}$  are comparable to values observed in other homologous derives.<sup>[2,3]</sup>

Figure 3 displays a projection in the (a, b) plane of the inorganic layer. In fact, it shows that the  $[\text{SO}_4]^{2-}$  groups and the octahedron are connected by three strong hydrogen bonds such as O1W-H1WA...O3<sup>i</sup>, O1W-H1WB...O4 and O4W-H4WA...O2<sup>iii</sup> and five weak hydrogen bonds to form infinite parallel bidimensional chains. These data reveal that each anion  $[\text{SO}_4]^{2-}$  is connected to four cations via eight water molecules.

In the organic molecule, there are  $\pi$ - $\pi$  interactions between antiparallel cations, with face-to-face distances of 3.070 Å.<sup>[30]</sup> Therefore, these interactions show a large role in the structure cohesion since they link two organic groups in the same layer (Figure 4). The examination of

**TABLE 3** Fractional atomic coordinates and isotropic or equivalent isotropic displacement parameters (Å<sup>2</sup>)

	x	y	z	Uiso*/Ueq
Ni	0.773 (6)	0.127 (5)	0.806 (3)	0.021 (17)
S	1.248 (12)	0.130 (10)	0.747 (6)	0.022 (2)
O1	1.329 (4)	0.064 (3)	0.697 (19)	0.033 (8)
O2	1.339 (4)	0.234 (3)	0.795 (2)	0.034 (8)
O3	1.118 (4)	0.200 (3)	0.703 (19)	0.030 (8)
O4	1.202 (4)	0.021 (3)	0.794 (18)	0.031 (8)
O1W	0.918 (4)	−0.020 (4)	0.792 (3)	0.044 (11)
O2W	0.837 (4)	0.237 (4)	0.722 (2)	0.030 (8)
O3W	0.625 (5)	0.024 (4)	0.726 (2)	0.032 (8)
O4W	0.626 (5)	0.279 (4)	0.812 (3)	0.054 (14)
N1	0.721 (4)	0.021 (4)	0.895 (2)	0.026 (8)
N2	0.917 (4)	0.220(4)	0.893(2)	0.026 (8)
C1	0.623 (6)	−0.079 (5)	0.891 (3)	0.029 (10)
C2	0.591 (6)	−0.145 (5)	0.953 (3)	0.034 (12)
C3	0.666 (6)	−0.096 (5)	1.022 (3)	0.036 (12)
C4	0.768 (6)	0.006 (5)	1.027 (3)	0.033 (11)
C5	0.795 (5)	0.065 (4)	0.962 (3)	0.027 (10)
C6	0.905 (5)	0.175 (4)	0.962 (3)	0.026 (10)
C7	0.992 (6)	0.230 (5)	1.025 (3)	0.034 (11)
C8	1.094 (6)	0.332 (5)	1.020 (3)	0.034 (12)
C9	1.108 (6)	0.376 (5)	0.950 (3)	0.033 (11)
C10	1.017 (6)	0.316 (5)	0.889 (3)	0.030 (11)
C11	0.482 (7)	−0.260 (6)	0.944 (4)	0.048 (15)
H1WA	0.914 (7)	−0.104 (6)	0.795 (3)	0.037 (15)*
H1WB	0.998 (7)	−0.010 (6)	0.791 (3)	0.035 (16)*
H2WA	0.900 (8)	0.222 (6)	0.711 (3)	0.038 (19)*
H2WB	0.829 (8)	0.325 (7)	0.724 (3)	0.060 (2)*
H3WA	0.553 (8)	0.040 (6)	0.719 (3)	0.040 (2)*
H3WB	0.634 (8)	−0.062 (8)	0.714 (4)	0.060 (2)*
H4WA	0.558 (9)	0.268 (8)	0.810 (4)	0.060 (3)*
H4WB	0.639 (8)	0.368 (8)	0.807 (4)	0.070 (2)*
H1	0.581 (6)	−0.098 (5)	0.844 (3)	0.021 (12)*
H3	0.646 (7)	−0.144 (6)	1.062 (3)	0.044 (15)*
H4	0.810 (7)	0.035 (6)	1.070 (3)	0.041 (16)*
H7	0.971 (6)	0.194 (5)	1.071 (3)	0.035 (14)*
H8	1.152 (7)	0.361 (5)	1.062 (3)	0.033 (14)*
H10	1.020 (6)	0.341 (5)	0.840 (3)	0.024 (12)*
H11A	0.474	−0.294	0.992	0.073*
H11B	0.513	−0.336	0.916	0.073*
H11C	0.391	−0.226	0.917	0.073*
H12A	1.273	0.512	0.988	0.067*

(Continues)

TABLE 3 (Continued)

	x	y	Z	Uiso*/Ueq
H12B	1.172	0.561	0.913	0.067*
H12C	1.284	0.440	0.913	0.067*

TABLE 4 Atomic displacement parameters ( $\text{\AA}^2$ )

Atoms	U <sup>11</sup>	U <sup>22</sup>	U <sup>33</sup>	U <sup>12</sup>	U <sup>13</sup>	U <sup>23</sup>
Ni	0.015(3)	0.014(3)	0.033(3)	-0.0007(2)	0.0063(2)	0.0006(2)
S	0.015(6)	0.014(5)	0.039(6)	-0.0004(4)	0.0092(5)	0.0003(4)
N1	0.025(3)	0.019(2)	0.036(2)	-0.0011(1)	0.0069(2)	0.0008(2)
N2	0.021(2)	0.021(2)	0.038(2)	-0.0012(1)	0.0037(2)	0.0009(2)
O1	0.028(2)	0.028(2)	0.049(2)	0.0065(1)	0.073(2)	-0.0013(1)
O2	0.025(2)	0.021(2)	0.056(2)	-0.0087(1)	0.0092(2)	-0.0041(1)
O3	0.017(2)	0.024(2)	0.049(2)	0.0075(1)	0.0076(2)	0.0031(1)
O4	0.029(2)	0.020(2)	0.044(2)	-0.0038(1)	0.0096(2)	0.0040(1)
O1W	0.023(2)	0.015(2)	0.100(3)	0.0012(1)	0.028(2)	-0.0034(2)
O2W	0.027(2)	0.022(2)	0.045(2)	-0.0051(1)	0.0121(2)	0.0029(1)
O3W	0.027(2)	0.022(2)	0.045(2)	-0.0051(1)	0.0121(2)	0.0029(1)
O4W	0.023(3)	0.016(2)	0.125(4)	0.0037(1)	0.024(3)	0.001(2)
C1	0.022(3)	0.029(2)	0.038(3)	-0.0050(2)	0.007(2)	0.0004(2)
C2	0.033(3)	0.024(2)	0.050(3)	0.0007(2)	0.016(3)	0.006(2)
C3	0.037(4)	0.037(3)	0.041(3)	0.000(2)	0.017(3)	0.008(2)
C4	0.034(3)	0.034(3)	0.034(3)	0.000(2)	0.010(2)	0.001(2)
C5	0.022(3)	0.024(2)	0.037(2)	0.0026(2)	0.009(2)	0.0002(2)
C6	0.020(3)	0.021(2)	0.037(2)	0.0051(2)	0.006(2)	0.0001(2)
C7	0.032(3)	0.038(3)	0.032(2)	-0.001(2)	0.005(2)	-0.002(2)
C8	0.027(3)	0.031(3)	0.043(3)	-0.0039(2)	0.003(3)	-0.010(2)
C9	0.025(3)	0.025(2)	0.048(3)	0.0018(2)	0.006(6)	-0.004(2)
C10	0.026(3)	0.029(2)	0.036(2)	-0.0043(2)	0.006(2)	0.0022(2)
C11	0.044(4)	0.040(3)	0.067(4)	-0.013(2)	0.022(3)	0.007(3)
C12	0.029(4)	0.042(3)	0.061(2)	-0.016(2)	0.005(3)	-0.005(3)

the geometrical features of the organic moiety indicates that the distance C-C and C-N varies between [1.375(7)-1.505(7)], [1.331(6)-1.360(6)], respectively. The mid-planes of organic groups are located at a  $z = 0$  and  $z = 0.5$  (Figure 5). These results are comparable to those similar  $[\text{Fe}(\text{C}_{12}\text{H}_{12}\text{N}_2)(\text{H}_2\text{O})_4]\text{SO}_4$  and  $[\text{Zn}(\text{C}_{12}\text{H}_{12}\text{N}_2)(\text{H}_2\text{O})_4]\text{SO}_4$  compounds.<sup>[21,22]</sup>

All the oxygen atoms of the  $\text{SO}_4$  are hydrogen bonded to water molecules. The S-O distances vary from 1.473(3) to 1.477(3)  $\text{\AA}$  and the O-S-O angles range between 109.1(2) and 110.2(2). These values confirm the distortion of the tetrahedron  $\text{SO}_4$ . The distances and angles of the

sulfate groups are quoted in Table 5. The present geometrical characteristics are usually comparable to those observed in some sulfate compounds.<sup>[31,32]</sup>

### 3.2 | X-ray powder diffraction (XRD) at room temperature

The lattice parameter and space group of  $[\text{Ni}(\text{C}_{12}\text{H}_{12}\text{N}_2)(\text{H}_2\text{O})_4]\text{SO}_4$  were investigated by Rietveld refinement using Fullprof program integrated in WinPLOTR software.<sup>[33,34]</sup> The material crystallises in the space group  $P2_1/c$  with the following unit cell parameters  $a =$

**TABLE 5** Geometric parameters (Å, °)

Ni—O1W	2.023 (3)	C4—C3	1.375 (7)
Ni—O4W	2.032 (4)	C5—C4	1.387 (6)
Ni—N2	2.058 (4)	C5—C6	1.475 (6)
Ni—O3W	2.061 (4)	C7—C6	1.387 (7)
Ni—O2W	2.063 (3)	C8—C9	1.382 (7)
Ni—N1	2.065 (3)	C8—C7	1.390 (7)
S—O3	1.473 (3)	C9—C10	1.376 (7)
S—O4	1.475 (3)	C12—C9	1.505 (7)
S—O2	1.476 (3)	O2W—H2WB	0.840 (7)
S—O1	1.477 (3)	O2W—H2WA	0.700 (6)
N1—C1	1.331 (6)	O1W—H1WA	0.800 (6)
N1—C5	1.351 (6)	O1W—H1WB	0.770 (6)
N2—C10	1.340 (6)	O3W—H3WB	0.860 (7)
N2—C6	1.360 (6)	O3W—H3WA	0.690 (7)
C1—C2	1.391 (6)	O4W—H4WB	0.860 (8)
C2—C3	1.391(8)	O4W—H4WA	0.650 (8)
C2—C11	1.493 (7)		
O1W—Ni—N2	92.80 (17)	O3—S—O1	109.60 (2)
O1W—Ni—O3W	86.98 (18)	O4—S—O1	109.21 (18)
O1W—Ni—O2W	86.84 (17)	O2—S—O1	110.20 (2)
O1W—Ni—N1	92.67 (16)	C1—N1—C5	119.10 (4)
O2W—Ni—N1	176.58 (17)	C1—N1—Ni	127.00 (3)
O3W—Ni—N1	95.23 (15)	C1—C2—C11	120.70 (5)
O3W—Ni—O2W	88.12 (15)	C3—C2—C1	115.70 (5)
O4W—Ni—N2	90.08 (19)	C3—C2—C11	123.60 (5)
O4W—Ni—O2W	89.33 (19)	C3—C4—C5	119.80 (5)
O4W—Ni—O3W	90.40 (2)	C4—C3—C2	120.70 (5)
O4W—Ni—N1	91.30 (18)	C4—C5—C6	123.50 (5)
N2—Ni—O3W	175.42 (14)	C5—N1—Ni	113.90 (3)
N2—Ni—O2W	96.44 (15)	C6—N2—Ni	114.20 (3)
N2—Ni—N1	80.20 (15)	C6—C7—C8	120.20 (5)
N2—C6—C7	120.30 (4)	C7—C6—C5	124.20 (4)
N2—C6—C5	115.50 (4)	C8—C9—C12	121.80 (5)
N2—C10—C9	124.30 (4)	C9—C8—C7	119.20 (5)
N1—C5—C4	120.30 (5)	C10—C9—C8	117.60 (5)
N1—C5—C6	116.20 (4)	C10—C9—C12	120.50 (5)
N1—C1—C2	124.40 (5)	C10—N2—C6	118.40 (4)
O3—S—O4	109.10 (2)	C10—N2—Ni	127.50 (3)
O3—S—O2	109.70 (2)		

9.552 Å,  $b = 9.591$  Å,  $c = 18.525$  Å and  $\beta = 104.215^\circ$ . The calculated diagram is in good agreement with the observed pattern. At room temperature, this result

exhibits the existence of a single phase and confirms its purity. At room temperature, the X-Ray diffractogram, of the title compound is indicated in Figure 6.

**TABLE 6** Calculated vibrational wavenumbers, measured infrared and Raman band position ( $\text{cm}^{-1}$ ) with the proposed assignments

IR	RAMAN	calculated	Attribution
3424(vs)	–	3517	$\nu(\text{OH}) + \nu(\text{CH})$
2964(w)	–	3037	$\nu(\text{OH}) + \nu(\text{CH})$
2926(w)	2919(w)	–	$\nu_{\text{as}}(\text{CH}_3)$
2742(w)	–	–	$\nu_{\text{as}}(\text{CH}_3)$
2544(w)	–	–	$\nu_{\text{s}}(\text{CH}_3)$
1608(s)	1592(vs)	1623	$\nu(\text{C}=\text{C})$
1499(m)	1490(vs)	1512	$\nu(\text{C}=\text{N})$
1477(vs)	–	1494	$\nu(\text{C}=\text{C})$
1454(m)	–	1462	$\delta_{\text{as}}(\text{CH}_3)$
1393(s)	1372(m)	1408	$\delta_{\text{s}}(\text{CH}_3)$
1312(m)	1308(s)	1335	$\delta_{\text{s}}(\text{CH}_3) + \delta(\text{C} - \text{H})$
1250(m)	1274(s)	1267	$\delta_{\text{s}}(\text{OH})$
1234(m)	1220(s)	1227	$\nu(\text{C}=\text{N}) + \delta(\text{C} - \text{H})$
1141(w)	1152(m)	1163	$\delta(\text{C} - \text{C} - \text{H}) + \nu_3(\text{SO}_4)$
1077(vs)	1037(w)	1063	$\nu_3(\text{SO}_4) + \rho(\text{CH}_3)$
997(w)	970(m)	983	$\nu_1(\text{SO}_4) + \gamma(\text{CH}_3)$
922(w)	–	966	$\gamma(\text{O-H})$
842(s)	–	873	$\gamma(\text{C-H})$
731(s)	751(w)	770	$\gamma(\text{C-H}) + \gamma(\text{C} = \text{C} - \text{C})$
700(s)	–	733	$\gamma\text{C} = \text{C} - \text{C}$
654(s)	685(w)	689	$\tau(\text{CCCC}) + \nu_4(\text{SO}_4)$
619(s)	647(w)	630	$\nu_4(\text{SO}_4)$
491(w)	–	502	$\gamma(\text{C} - \text{C} = \text{N}) + \gamma(\text{C} = \text{C} - \text{C})$
419(s)	420(w)	414	$\nu_2(\text{SO}_4)$

vs: very strong. s: strong. m: medium. w: weak.  $\nu$ : stretching.  $\nu_{\text{a}}$ : asymmetric stretching.  $\nu_{\text{s}}$ : symmetric stretching.  $\delta$ : in the plane bending.  $\gamma$ : out of plane bending.  $\tau$ : twisting.  $\rho$ : rocking.

### 3.3 | Thermal behavior

The thermal decomposition of complex  $[\text{Ni}(\text{C}_{12}\text{H}_{12}\text{N}_2)(\text{H}_2\text{O})_4]\text{SO}_4$  was studied using thermogravimetric measurements and differential scanning calorimetric (Figure 7). The TG curve exhibits two distinct steps, at 118 °C–250 °C and from 400 °C to around 460 °C. The first step corresponding to the dehydration of the precursor occurs in two steps. The first loss, between 118 and 163 °C (observed weight loss, 4.28%; calculated weight loss, 4.37%), is attributed to the elimination of one water molecule. The second loss, between 163 °C and 250 °C (observed weight loss, 13.02%; theoretical, 13.13%), is ascribed to the departure of the remaining water molecules leading to the formation of the anhydrous phase. DTA curves display three endothermic peaks, at 154, 196 and 468 °C. The two first peaks corresponding to the dehydration of  $[\text{Ni}(\text{C}_{12}\text{H}_{12}\text{N}_2)(\text{H}_2\text{O})_4]\text{SO}_4$  and the third peak corresponding to the second step in the TG

curves, which indicates the decomposition of the amine entity.

### 3.4 | Vibrational study

In order to yield more information about this compound, we have undertaken the Raman scattering and infrared absorption between 400 and 4000  $\text{cm}^{-1}$ , at room temperature. The experimental IR and Raman wavenumbers compared to the calculated from DFT method are shown in Table 6 along with detailed assignments.

For visual comparison, the observed and simulated IR and Raman spectra of the  $[\text{Ni}(\text{dmpy})(\text{H}_2\text{O})_4]\text{SO}_4$  are given in Figure 8 and Figure 9. All the bands observed were assigned by comparison with the spectrum of other compounds.<sup>[35–43]</sup> All the IR and Raman bands of this crystal observed in the region below 300  $\text{cm}^{-1}$  must be due to external vibrations.

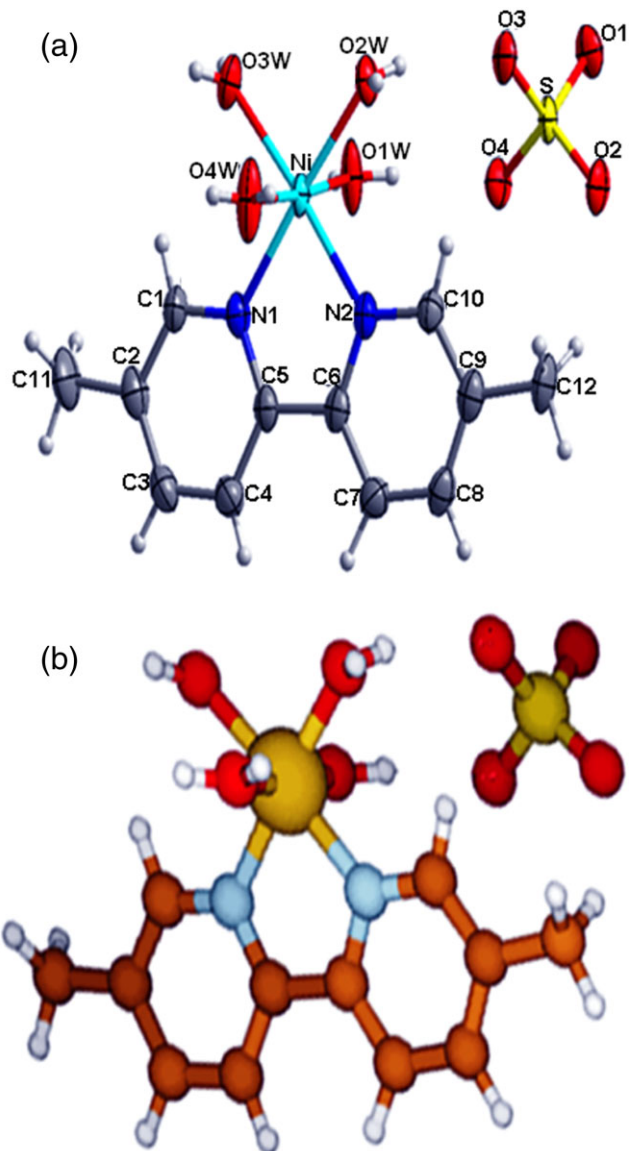


**FIGURE 2** (a) Asymmetric unit of the  $[\text{Ni}(\text{C}_{12}\text{H}_{12}\text{N}_2)(\text{H}_2\text{O})_4]\text{SO}_4$  crystal. (b) Optimized geometry of the  $[\text{Ni}(\text{C}_{12}\text{H}_{12}\text{N}_2)(\text{H}_2\text{O})_4]\text{SO}_4$

### 3.4.1 | Vibration of $[\text{SO}_4]^{2-}$ anion

According to the literature, we have attributed the vibrational modes of the anion  $\text{SO}_4^{2-}$ .<sup>[35–39]</sup> The presence of sulfate anions in the crystal structure of  $[\text{Ni}(\text{C}_{12}\text{H}_{12}\text{N}_2)(\text{H}_2\text{O})_4]\text{SO}_4$  is manifested in the IR spectrum by two bands of the asymmetric stretching vibration  $\nu_3$ , the first weak one at  $1141\text{ cm}^{-1}$  and the second very strong peak at  $1077\text{ cm}^{-1}$ , and appeared in Raman around  $1152$  and  $1037\text{ cm}^{-1}$ . This mode appears in our DFT calculation at  $1163$  and  $1063\text{ cm}^{-1}$ . In IR, there is a small band at  $997\text{ cm}^{-1}$  on the symmetric stretching vibration  $\nu_1$  of  $\text{SO}_4^{2-}$ , also detected in Raman around  $960\text{ cm}^{-1}$ . The symmetric  $\nu_2$  and asymmetric  $\nu_4$  modes of deformation are noted as two bands at  $491$ ,  $419\text{ cm}^{-1}$  and  $654$ ,  $619\text{ cm}^{-1}$ , respectively. The DFT calculations expected these modes at  $414$  and  $630\text{ cm}^{-1}$ .

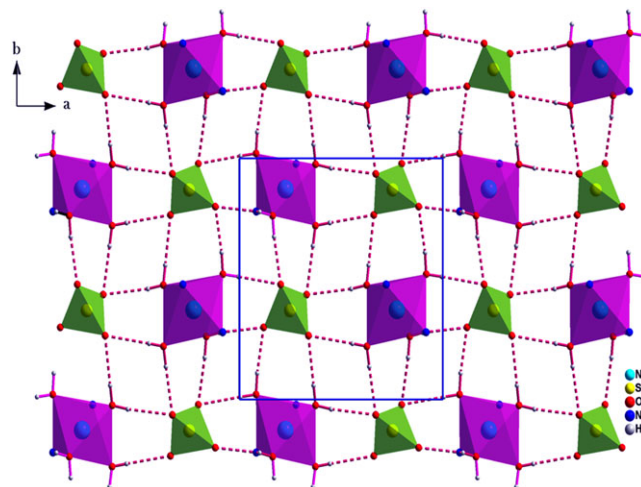


**FIGURE 3** Two-dimensional sheet in the  $ab$  plane where ions are linked via classical  $\text{O-H}\cdots\text{O}$  hydrogen bonds in  $[\text{Ni}(\text{C}_{12}\text{H}_{12}\text{N}_2)(\text{H}_2\text{O})_4]\text{SO}_4$

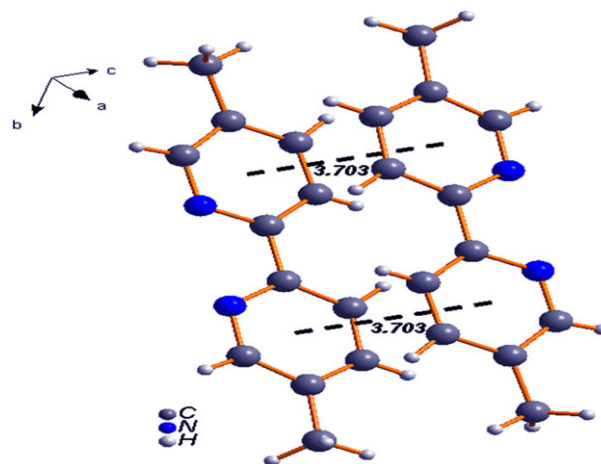


**FIGURE 4** Offset-face-to-face interactions motifs in the cation layer

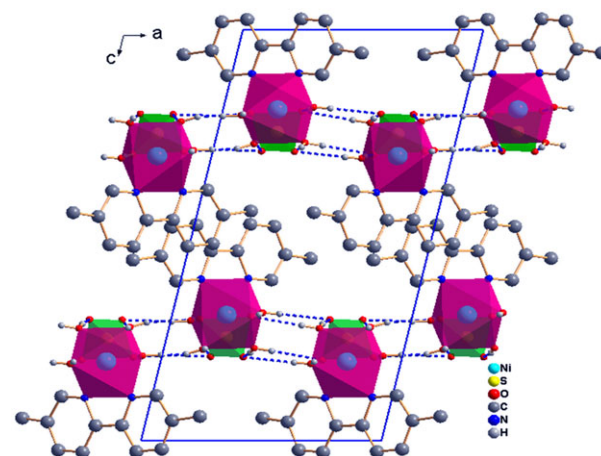


**FIGURE 5** The atomic arrangement of  $[\text{Ni}(\text{C}_{12}\text{H}_{12}\text{N}_2)(\text{H}_2\text{O})_4]\text{SO}_4$  in projection along the  $b$ -axis

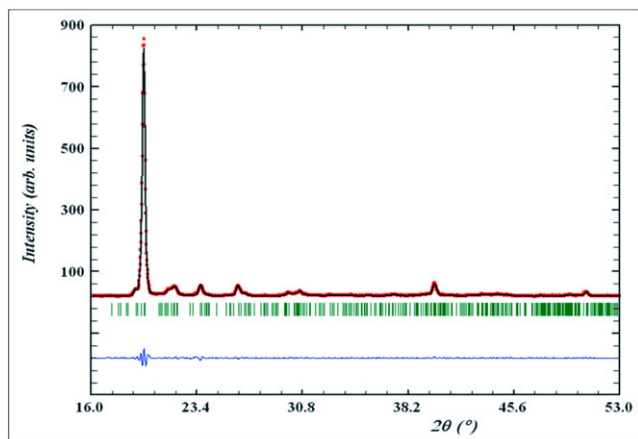


**FIGURE 6** Rietveld refinement of the X-ray diffraction powder pattern of  $[\text{Ni}(\text{C}_{12}\text{H}_{12}\text{N}_2)(\text{H}_2\text{O})_4]\text{SO}_4$

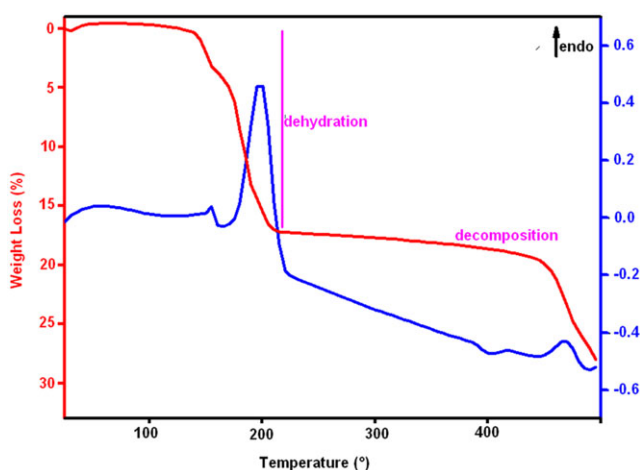


**FIGURE 7** Thermogravimetric and differential thermal analysis plot for  $[\text{Ni}(\text{C}_{12}\text{H}_{12}\text{N}_2)(\text{H}_2\text{O})_4]\text{SO}_4$

### 3.4.2 | The vibration of water molecule

The complex  $[\text{Ni}(\text{dmpy})(\text{H}_2\text{O})_4]\text{SO}_4$  exhibits a broad, structured, strong band ranging from  $3100$  to  $3400\text{ cm}^{-1}$ .<sup>[35,36,38]</sup> This band is in agreement with the presence of water molecules, involved in the system of hydrogen bonds (as can be seen from the hydrogen bonding table). The out-of-plane bending mode  $\gamma(\text{OH})$  appears in IR at  $922\text{ cm}^{-1}$ , but it is not observed in spectra Raman. This mode shows a good agreement with predicted DFT calculation at  $966\text{ cm}^{-1}$ . In IR, the deformation modes in the plane  $\delta(\text{OH})$  appear around  $1250\text{ cm}^{-1}$ , for DFT calculation, appear at  $1308\text{ cm}^{-1}$ .

### 3.4.3 | The vibration of organic motif

Generally, in the cation, 5,5'-dimethyl-2,2'-bipyridine the aromatic C-H stretching vibration groups  $\nu(\text{C}_{\text{aromatic}}-\text{H})$  are detected in the region located between  $3000$  and  $3450\text{ cm}^{-1}$ .<sup>[42]</sup> For the crystal under study, these modes are

observed by two bands occurring at  $3424$  and  $2964\text{ cm}^{-1}$  in the experimental infrared spectra, but they are not observed in Raman spectra. The bands, which appear at  $1308$ , and  $1220\text{ cm}^{-1}$  in Raman spectra, correspond to the in-plane bending mode  $\gamma(\text{C-H})$ . These vibrations are noted in IR at  $1312$ , and  $1234\text{ cm}^{-1}$ . The DFT calculations determined this mode at  $1335$ , and  $1227\text{ cm}^{-1}$ . The very weak band, at  $2926$  and  $2742\text{ cm}^{-1}$  in IR spectra, is attributed to  $\text{CH}_3$  asymmetric stretching. This mode appears in Raman spectra at  $2919\text{ cm}^{-1}$ . The symmetric bands  $\nu_s(\text{CH}_3)$  are located at  $2544\text{ cm}^{-1}$  with weak intensity in FT-IR spectrum. From the theoretical calculations, the symmetric bending vibrations  $\delta_s(\text{CH}_3)$  are predicted at  $1408$  and  $1335\text{ cm}^{-1}$ . It shows excellent correlation with the FT-IR and FT-Raman bands at  $1393$  and  $1312$ , and  $1372$   $1308\text{ cm}^{-1}$ , respectively.

According to our previous results,<sup>[40-43]</sup> the stretching modes of the bands C=C and C=N of the pyridine ring are observed in the region between  $1650$ - $1400\text{ cm}^{-1}$ . In our case, we noted a strong band in the FT-IR spectrum at  $1608\text{ cm}^{-1}$  and a very high intensity peak at  $1477\text{ cm}^{-1}$ , assigned to C=C stretching vibrations. In Raman spectrum, this mode is observed at  $1592\text{ cm}^{-1}$ . The DFT computation predicts this vibrational mode at  $1623\text{ cm}^{-1}$  and  $1462\text{ cm}^{-1}$ . On the other hand, the stretching modes of C=N is traced at  $1499$ ,  $1234\text{ cm}^{-1}$  and  $1490$ ,  $1220\text{ cm}^{-1}$  in both IR and Raman, respectively. The computed DFT frequencies for the ring vibrational modes indicate excellent agreement with the experimental data of the title compound.

## 3.5 | Optical properties

The UV-Vis absorption spectra recorded in the  $200$ - $800\text{ nm}$  range are displayed in Figure 10. As expected, the spectra exhibit four absorption bands; the two first absorption bands are at  $255$  and  $269\text{ nm}$  corresponding to  $\pi$ - $\pi^*$  transitions in dmpy ligand. The last two absorption bands are at  $287$  and  $319\text{ nm}$ , which could be attributed to  $n$ - $\pi^*$  transition. The value of the optical band gap of the compound is  $1.89\text{ eV}$  (Figure 11), which could be a sign of their semiconductor nature (the values of  $E_g$  were obtained by the use of a straightforward extrapolation method).

## 3.6 | Catalytic reactivity Study:

The  $[\text{Ni}(\text{C}_{12}\text{H}_{12}\text{N}_2)(\text{H}_2\text{O})_4]\text{SO}_4$  complex was tested as a catalyst for the coupling reactions of Heck and copper-free Sonogashira under ultrasonic irradiation in the presence of different bases in various solvents. At a first stage, we studied the effect of solvent on the reactivity of the coupling reaction of styrene with chlorobenzene. The results obtained are given in Table 7. It is noted that the evolution of the reaction increases with the polarity

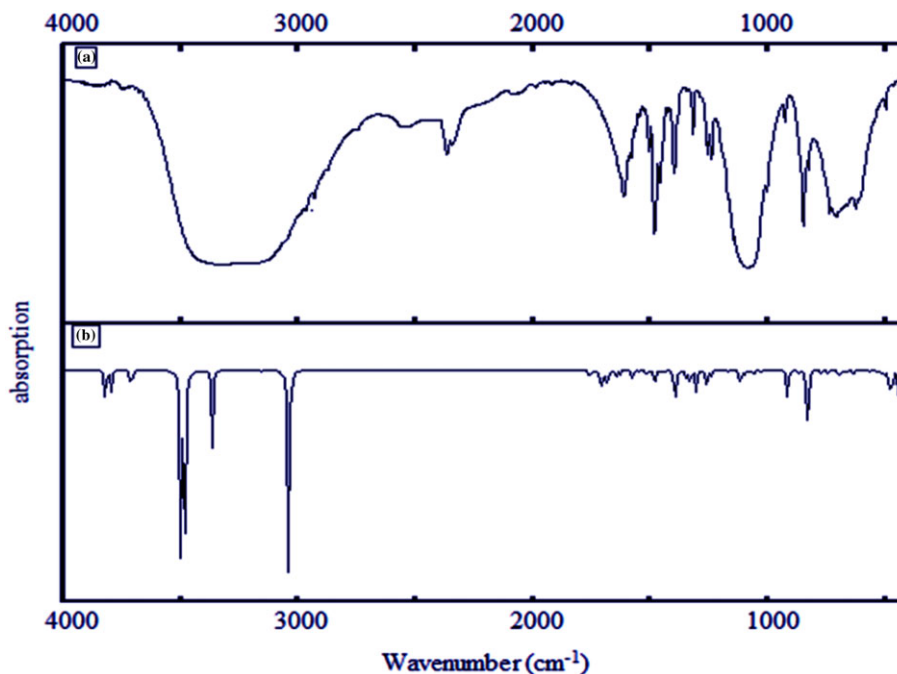


**FIGURE 8** (a) Experimental IR spectrum and (b) simulated IR spectrum of the  $\text{Ni}(\text{C}_{12}\text{H}_{12}\text{N}_2)(\text{H}_2\text{O})_4]\text{SO}_4$

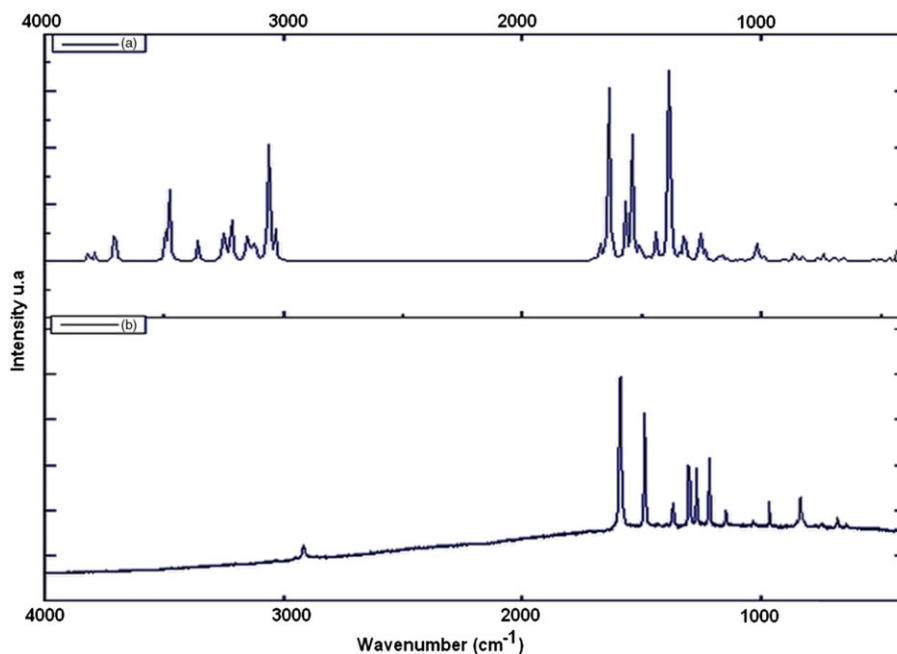


**FIGURE 9** (a) Simulated Raman spectrum and (b) experimental Raman spectrum of the  $\text{Ni}(\text{C}_{12}\text{H}_{12}\text{N}_2)(\text{H}_2\text{O})_4]\text{SO}_4$

of the solvent. The use of DMSO, DMF and MeCN induced good yields reaching 95%, 86% and 58%, respectively (entry 1, 3 and 7). However, the use of  $\text{H}_2\text{O}$  and THF results in low yields of 19% and 20% for longer time duration: 45 min (entry 5 and 6). This can be explained by the secondary reactions which may occur in an aqueous medium.<sup>[44]</sup> In addition, solvents having low boiling temperatures, such as THF, involve rapid vaporization during the reaction. Thus, the decrease in liquid level

minimizes the solvation of the reagents and increases the cavitation threshold.<sup>[45]</sup> If we examine the influence of the nature of the base, we find that  $\text{NaCO}_3$  is best suited to affect the coupling of styrene with chlorobenzene (entry 1 and 3). However, the addition of  $\text{Bu}_3\text{N}$  and  $\text{NaOH}$  induces much lower yields (entry 2 and 4).

In order to elucidate the formation of the different products obtained, we suggest the reaction mechanism proposed in Figure 12.

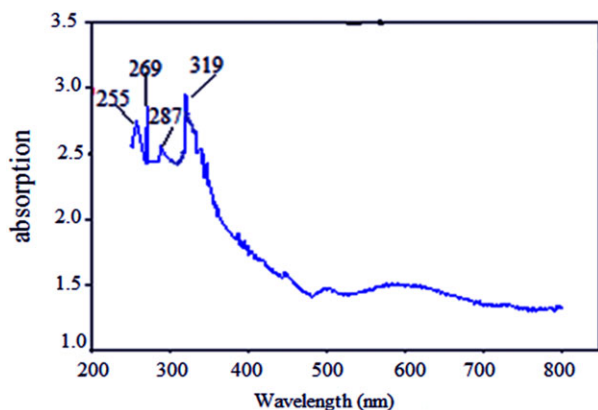


**FIGURE 10** UV-Vis absorption spectrum of the  $[\text{Ni}(\text{C}_{12}\text{H}_{12}\text{N}_2)(\text{H}_2\text{O})_4]\text{SO}_4$

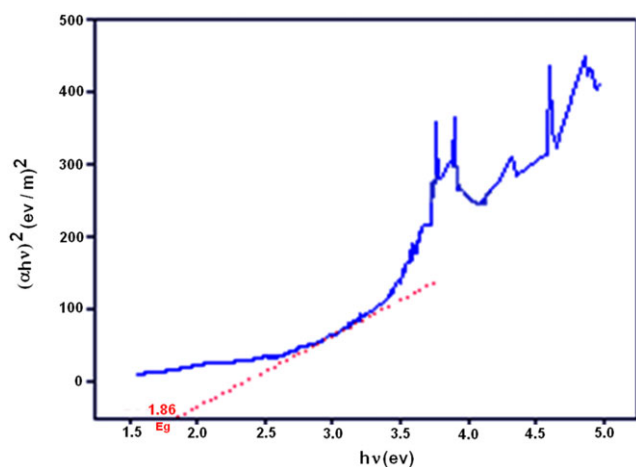


**FIGURE 11** Determination of the optical band gap of  $[\text{Ni}(\text{C}_{12}\text{H}_{12}\text{N}_2)(\text{H}_2\text{O})_4]\text{SO}_4$  by UV-Vis absorption spectrum

The cycle begins with the oxidative addition of the aryl halide to the initial complex; followed by the syn-insertion of styrene to the complex formed which generates

the formation of a new unstable C-C bond (3).<sup>[46]</sup> This involves an internal rotation around this bond so that the hydrogen in  $\beta$  of the metal center becomes in the syn position relative to Ni and thus promotes a  $\beta$ -elimination which generates the stilbene and the hydride (5). Finally, the presence of the base decomposes this hydride by regenerating the initial complex and trapping the HX acid formed.

The study of the coupling reaction of chlorobenzene with phenylacetylene in the presence of  $[\text{Ni}(\text{C}_{12}\text{H}_{12}\text{N}_2)(\text{H}_2\text{O})_4]\text{SO}_4$  as catalyst displays moderate to high yields (Table 8). The use of inorganic bases, such as  $\text{Na}_2\text{CO}_3$  (entry 1), induces a slightly lower reactivity than that obtained in the presence of  $\text{Bu}_3\text{N}$  and  $\text{Et}_3\text{N}$  (entry 2 and 3). This is consistent with  $\text{NaOH}$  which induces null results even after a period of 45 minutes (entry 4 and 7).

Among the solvents examined, it appears that DMF is most suitable for this type of coupling. Thus, the yield reached 73% in a short time (30 min).

In order to interpret these results, we have explained the phenomenon of cavitation due to ultrasonic irradiation as indicated in Figure 13. Indeed, the creation of the ultrasonic wave within the reaction medium increases the possibility of contact between the reagents.<sup>[47]</sup> This generates the pressure variation in the reaction mixture. These differences in pressure imply distensions and approximations between the molecular groups.<sup>[46,48]</sup> During the rarefaction cycle, the distance between these groups increases the cohesive forces in the liquid, which are overcome. The presence of the dissolved gases and the liquid vapor generate the appearance of microbubbles called cavitation bubbles. These bubbles undergo compression and decompression forces implying that by their enlargement at a maximum size these

**TABLE 7** Coupling of chlorobenzene with styrene in presence of  $[\text{Ni}(\text{C}_{12}\text{H}_{12}\text{N}_2)(\text{H}_2\text{O})_4]\text{SO}_4$

Entry	Solvent	Base	Time (min)	Yield (%) <sup>a</sup> E/Z
1	DMSO	$\text{Na}_2\text{CO}_3$	30	95/<1
2	DMSO	$\text{Bu}_3\text{N}$	30	35/3
3	DMF	$\text{Na}_2\text{CO}_3$	30	86/9
4	DMF	$\text{NaOH}$	30	37/11
5	$\text{H}_2\text{O}$	$\text{Na}_2\text{CO}_3$	45	19/12
6	THF	$\text{Na}_2\text{CO}_3$	45	20/1
7	MeCN	$\text{Na}_2\text{CO}_3$	30	58/5

0.012 mmol of catalyst, 1.5 mmol of base, 1 mmol of aryl halide, 1 mmol of styrene, 6 mL of solvent, US, 25 °C. <sup>a</sup> the yields were measured by GC using dichloromethane as solvent

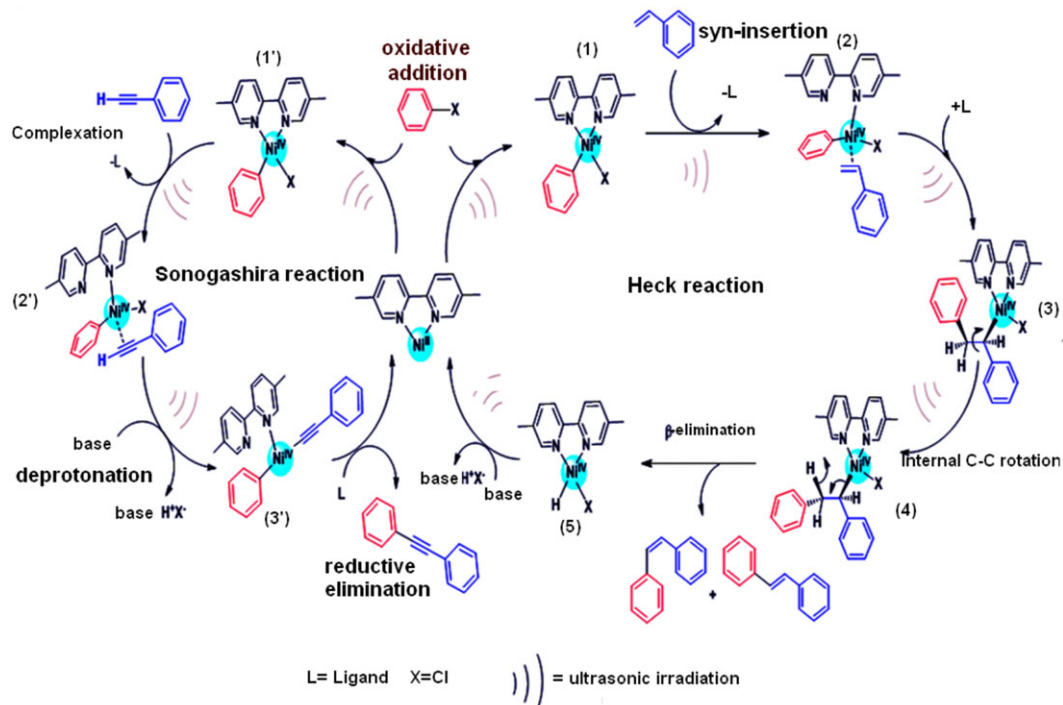


**FIGURE 12** Proposed catalytic mechanism of the Heck and Sonogashira coupling reaction catalysed by  $[\text{Ni}(\text{C}_{12}\text{H}_{12}\text{N}_2)(\text{H}_2\text{O})_4]\text{SO}_4$

**TABLE 8** Coupling of chlorobenzene with phenylacetylene in presence of  $[\text{Ni}(\text{C}_{12}\text{H}_{12}\text{N}_2)(\text{H}_2\text{O})_4]\text{SO}_4$

Entry	Solvent	Base	Time (min)	Yield (%) <sup>a</sup>
1	DMF	$\text{Na}_2\text{CO}_3$	30	45
2	DMF	$\text{Et}_3\text{N}$	30	59
3	DMF	$\text{Bu}_3\text{N}$	30	73
4	DMSO	$\text{NaOH}$	45	-
5	DMSO	$\text{Bu}_3\text{N}$	30	65
6	THF	$\text{Bu}_3\text{N}$	45	60
7	$\text{H}_2\text{O}$	$\text{NaOH}$	45	-
8	$\text{H}_2\text{O}$	$\text{Bu}_3\text{N}$	30	63

0.012 mmol of catalyst, 1.5 mmol of base, 1 mmol of aryl halide, 1 mmol of phenylacetylene, 6 mL of solvent, US, 25 °C. <sup>a</sup> the yields were measured by GC using dichloromethane as solvent.

cavitations become unstable.<sup>[49]</sup> The pressure variation indicates their collapse. All forces from the outside cause their implosion. The internal pressures due to the gas result in their explosion with enormous energy release within reaction medium. The low boiling temperature of THF conveys its rapid vaporization during the reaction. Hence, the decrease in liquid level greatly increases the cavitation rate in the medium which adversely affects the course of the reaction.

The catalytic cycle of the copper-free sonogashira reaction is not yet well known. The mechanism that we

suggested in Figure 12 is derived from a catalytic literature cycle that has recently been proposed.<sup>[50,51]</sup> The formation of the complex (1') by the oxidative addition of the aryl halide to the initial complex generates its complexation with phenylacetylene by the dissociation of one out of two nitrogen ligands (L) (2'). This increases the acidity of the phenylacetylene proton relative to its free state.<sup>[52]</sup> Therefore, the presence of the base favors its deprotonation which generates the complex (3'). This latter reduces the reductive elimination by yielding the diphenylacetylene and the regeneration of the initial state of the catalyst.

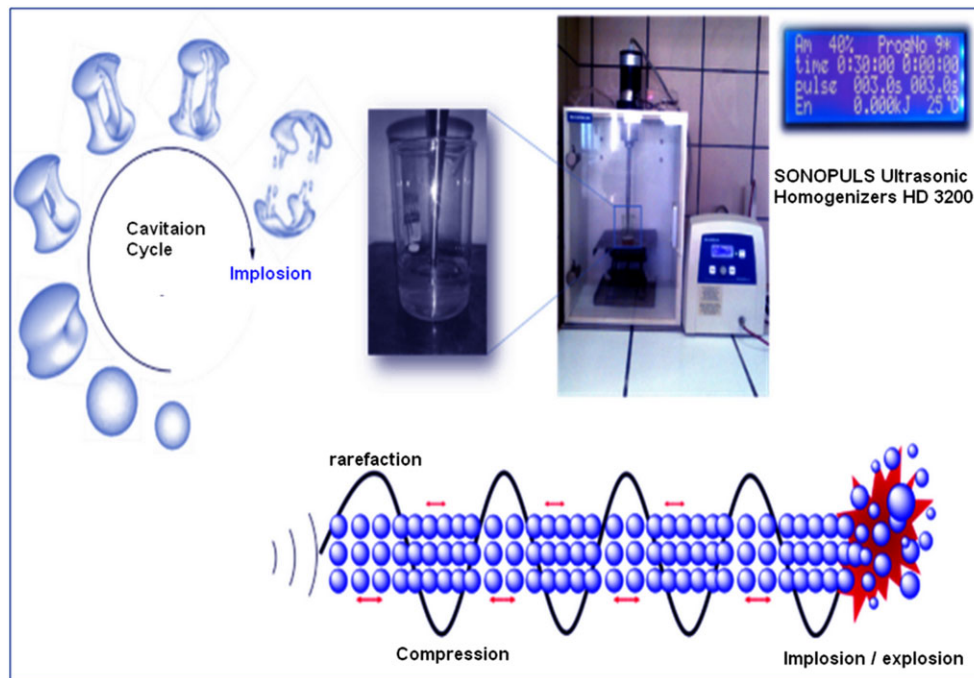


**FIGURE 13** Ultrasonic irradiation: creation of bubbles followed by their implosion/explosion

### 3.6.1 | (E)-1,2-diphenylethylene

Mp: 124–126 °C; IR (KBr,  $\text{cm}^{-1}$ )  $\nu$  = 2887–3000 (CH aro), 1594 (C=C ethyl), 1493 (C=C aro), 957 (CH ethyl);  $^1\text{H}$  NMR (400 MHz,  $\text{CDCl}_3$ )  $\delta$  (ppm) = 7.55 (d, 4H,  $J$  = 7.54 Hz), 7.39 (t, 4H,  $J$  = 7.4 Hz), 7.32–7.26 (m, 2H), 7.15 (s, 2H);  $^{13}\text{C}$  NMR (100 MHz,  $\text{CDCl}_3$ )  $\delta$  (ppm) = 131.6, 128.3, 128.2, 123.3, 89.4.

### 3.6.2 | Diphenylacetylene

Mp: 60–62 °C; IR (KBr,  $\text{cm}^{-1}$ )  $\nu$  = 2989–3121 (CH aro), 1853–1967 (C $\equiv$ C), 1487 (C=C aro);  $^1\text{H}$  NMR (400 MHz,  $\text{CDCl}_3$ )  $\delta$  (ppm) = 7.60–7.56 (m, 6H), 7.41–7.36 (m, 4H);  $^{13}\text{C}$  NMR (100 MHz,  $\text{CDCl}_3$ )  $\delta$  (ppm) = 137.3, 128.7, 128.6, 127.6, 126.5.

## 4 | CONCLUSIONS

The nickel (II) sulfate templated by dmpy with the formula  $[\text{Ni}(\text{C}_{12}\text{H}_{12}\text{N}_2)(\text{H}_2\text{O})_4]\text{SO}_4$  was prepared under hydrothermal conditions, characterized and discussed in this article. The crystal structure was resolved by X-ray single-crystal diffraction data. It consists of  $\text{Ni}^{2+}\text{O}_4\text{N}_2$  octahedra, sulfate tetrahedra, and 5,5'-dimethyl-2, 2'-bipyridine cations. These entities are assembled by one kind of hydrogen bonds O-H...O to form a three-dimensional structure. The thermal behavior studies are summarized by the elimination of water molecules and the decomposition of the anhydrous compound. Vibrational

study, determined by IR and Raman spectroscopy recorded in the frequency range 400–4000  $\text{cm}^{-1}$ , is very significant as it verifies the dependence of the entities constituting our compound. The computed DFT frequencies for the  $[\text{Ni}(\text{C}_{12}\text{H}_{12}\text{N}_2)(\text{H}_2\text{O})_4]\text{SO}_4$  show excellent agreement with the experimental data of the title compound. The catalytic study was tested in Heck and Sonogashira coupling reactions under ultrasonic irradiation. The results obtained reveal that the sonochemical activation yields a moderate to high yields for a short period of time, i.e. of just a few minutes (30–45 min).

## ACKNOWLEDGEMENTS

We are grateful to Mr. Tarek GARGOURI for access to the KAPPA CCD diffractometer. \*H.

## ORCID

Wassim Maalej  <http://orcid.org/0000-0002-8818-2085>

## REFERENCES

- [1] H. Wu, J. Zhou, H. Yu, L. Lu, Z. Xu, Y. Wan, D. Shi, *Acta Crystallogr. Sect. E* **2004**, 60, 822.
- [2] S. Suarez, F. Doctorovich, M. A. Harvey, R. Baggio, *Acta Crystallogr. Sect. C* **2013**, 69, 351.
- [3] S. Boonlue, C. Theppitak, K. Chainok, *Acta Crystallogr. Sect. E* **2012**, 68, m908.

- [4] F. Hajlaoui, S. Yahyaoui, T. Mhiri, T. Bataille, *Struct. Chem.* **2012**, *53*, 334.
- [5] L. F. Kirpichnikova, L. A. Shuvalov, N. R. Ivanov, B. N. Prasolov, E. F. Andreyev, *Ferroelectrics* **1989**, *96*, 313.
- [6] F. Hajlaoui, S. Yahyaoui, H. Naili, T. Mhiri, T. Bataill, *Inorg. Chim. Acta* **2010**, *363*, 691.
- [7] F. Hajlaoui, H. Naili, S. Yahyaoui, M. M. Turnbull, T. Mhiri, T. Bataille, *Dalton Trans.* **2011**, *40*, 11613.
- [8] N. Farkašová, J. Cernák, L. R. Falvello, M. Orendác, R. Boc, *Acta Crystallogr. Sect. C* **2015**, *71*, 252.
- [9] Q. Wang, H. Guo, S. Li, F. Gao, D. Fang, *J. Solution Chem.* **2009**, *38*, 1085.
- [10] D. B. Leznoff, N. D. Draper, R. Batchelor, *J. Polyhedron* **2003**, *22*, 1735.
- [11] R. L. LaDuca, M. P. Desciak, R. S. Rarig Jr, J. A. Zubieta, *Z. Anorg. Allg. Chem.* **2006**, *632*, 449.
- [12] H. Naïli, F. Hajlaoui, T. Mhiri, T. C. O. M. Leod, M. N. Kopylovich, K. T. Mahmudovb, A. J. L. Pombeiro, *Dalton Trans.* **2013**, *42*, 399.
- [13] K. T. Mahmudov, M. N. Kopylovich, M. F.C. G. da Silva and A. J. L. Pombeiro, *Dalton Trans.* **2017**, *46*, 10121-10138
- [14] D. R. Boyd, N. D. Sharma, L. Sbircea, D. Murphy, T. Belhocine, J. F. Malone, S. L. James, C. C. R. Allen, J. T. G. Hamilton, *Chem. Commun.* **2008**, 5535.
- [15] M. P. A. Lyle, P. D. Wilson, *Org. Biomol. Chem.* **2006**, *4*, 41.
- [16] A. V. Malkov, D. Pernazza, M. Bell, M. Bella, A. Massa, F. Teply, P. Meghani, P. J. Kocovsky, *Org. Chem.* **2003**, *68*, 4727.
- [17] G. Chelucci, A. Iuliano, D. Muroi, A. Saba, *J. Mol. Catal. A* **2003**, *191*, 29.
- [18] G. Chelucci, G. Loriga, G. Murineddu, G. A. Pinna, *Tetrahedron Lett.* **2002**, *43*, 3601.
- [19] Q. T. Tan, M. Hayashi, *Adv. Synth. Catal.* **2008**, *350*, 2639.
- [20] L. C. Liang, F. Y. Chen, M. H. Huang, L. C. Cheng, C. W. Lia, H. M. Lee, *Dalton Trans.* **2010**, *39*, 9941.
- [21] A. V. Malkov, I. R. Bexendale, M. Bella, V. Langer, J. Fawcett, D. R. Russell, D. J. Mansfield, M. Valko, P. Kocovsky, *Organometallics* **2001**, *20*, 673.
- [22] J. Niu, H. Zhou, Z. Li, *J. Org. Chem.* **2008**, *73*, 7814.
- [23] J. A. Terrett, J. D. Cuthbertson, V. W. Shurtleff, D. W. C. Mac-Millan, *Nature* **2015**, *524*, 330-334.
- [24] *International Tables for X-ray Crystallography*, Vol. C, Kluwer, Dordrecht **1992**.
- [25] L. J. Farrugia, *J. Appl. Crystallogr.* **1999**, *32*, 837.
- [26] G. M. Sheldrick, *SHELXS-86, Program for the Solution of Crystal Structure*, Univ. of Gottingen, Germany **1990**.
- [27] G. M. Sheldrick, *Acta Crystallogr. Sect. A* **2008**, *64*, 112.
- [28] K. Brandenburg, *Diamond Version 2.0*, Impact GbR, Bonn, Germany **1998**.
- [29] A. D. Becke, *J. Chern. Phys.* **1993**, *98*, 5648.
- [30] C. Janiak, *Dalton Trans.* **2000**, 3885.
- [31] Q.-L. Zhao, H.-F. Bai, *Acta Crystallogr. Sect. E* **2009**, *65*, 866.
- [32] Y. Belamri, F. Setifi, B. M. Francuski, S. B. Novakovic, S. Zouaoui, *Acta Crystallogr. Sect. E* **2014**, *70*, 544.
- [33] J. Rodriguez-Carvajal, *J. Program FULLPROF, version 2.6* **2005**, *1*.
- [34] T. Roisnel, J. Rodriguez-Carvajal, *Mater. Sci. Forum* **2001**, *268*, 378.
- [35] J. Cihelka, D. Havlicek, R. Gyepes, I. Němec, Z. Koleva, *J. Mol. Struct.* **2010**, *980*, 31.
- [36] C. Papatriantafyllopoulou, C. G. Efthymiou, C. P. Raptopoulou, R. Vicente, E. Manessi-Zoupa, V. Psycharis, A. Escuer, S. P. Perlepes, *J. Mol. Struct.* **2007**, *829*, 176.
- [37] M. Belhouchet, M. Bahri, J. M. Savariault, T. Mhiri, *Spectrochim Acta A* **2005**, *61*, 387.
- [38] W. Amamou, T. Guerfel, T. Mhiri, *CSTA* **2012**, *1*, 40.
- [39] C. Papatriantafyllopoulou, C. P. Raptopoulou, A. Terzisb, J. F. Janssensc, S. P. Perlepesa, E. Manessi-Zoupa, *Z. Naturforsch.* **2007**, *62b*, 1123.
- [40] S. Guidara, H. Feki, Y. Abid, *J. Mol. Struct.* **2015**, *1080*, 176.
- [41] R. Mani, I. B. Rietveld, K. Varadharajan, M. Louhi-Kultanen, S. Muthu, *J. Phys. Chem.* **2014**, *118(34)*, 6883.
- [42] V. Krishnakumar, L. Guru Prasad, R. Nagalakshmi, *Eur. Phys. J. Appl. Phys.* **2009**, *48*, 20403.
- [43] D. Fredj, C. Ben Hassen, S. Elleuch, H. Feki, N. Chniba-Boudjada, T. Mhiri, M. Boujelbene, *Mater. Res. Bull.* **2017**, *85*, 23.
- [44] H. Wang, H. Cheng, F. Zhao, *Green and Sustainable Chemistry* **2014**, *4*, 1.
- [45] T.J. Mason, J.P. Lorimer, Ellis Horwood limited. **1988**, 32.
- [46] D. Atoui, K. Said, R. Ben Salem, *Turk. J. Chem.* **2017**, *41*, 587.
- [47] K. Said, Y. Moussaoui, M. Kammoune, R. Ben Salem, *Ultrason. Sonochem.* **2011**, *18*, 23.
- [48] S. Veillet, V. Tomao, F. Chemat, *Food Chem.* **2010**, *123*, 905.
- [49] K. Said, R. Ben Salem, *Engineering and Science* **2016**, *6*, 111.
- [50] A. Tougerti, S. Negri, A. Jutand, *Chem. – Eur. J.* **2007**, *13*, 666.
- [51] A. Soheili, J. A. Walker, J. A. Murry, P. G. Dormer, D. L. Hughes, *Org. Lett.* **2003**, *5*, 4191.
- [52] X. Moreau, J. L. Campaign, G. Meyer, A. Jutand, *Eur. J. Org. Chem.* **2005**, 3749.

**How to cite this article:** Jaballi R, Maalej W, Atoui D, Feki H, Ben Salem R, Elaoud Z. Crystal packing, vibrational studies, DFT calculations of a new hybrid nickel (II)-complex and its application in Heck and Sonogashira cross-coupling reactions. *Appl Organometal Chem.* 2018;e4366. <https://doi.org/10.1002/aoc.4366>